Computer Science and Information Systems 20(4):1845–1868 https://doi.org/10.2298/CSIS221222033H

A^{2}FWPO: Anti-aliasing Filter Based on Whale Parameter Optimization Method for Feature Extraction and Recognition of Dance Motor Imagery EEG

Tianliang Huang[1,⋆], Ziyue Luo[1], and Yin Lyu[2]

[1] School of Art, Hunan University of Information Technology
Maotang Industrial Park, Changsha Economic and Technological Development Zone (410151) China
tlhuang2023@163.com
luoziyue77@163.com
[2] College of Music, Huaiyin Normal University
Huai'an, China
8201711037@hytc.edu.cn

Abstract. The classification accuracy of EEG signals based on traditional machine learning methods is low. Therefore, this paper proposes a new model for the feature extraction and recognition of dance motor imagery EEG, which makes full use of the advantage of anti-aliasing filter based on whale parameter optimization method. The anti-aliasing filter is used for preprocessing, and the filtered signal is extracted by two-dimensional empirical wavelet transform. The extracted feature is input to the robust support matrix machine to complete pattern recognition. In pattern recognition process, an improved whale algorithm is used to dynamically adjust the optimal parameters of individual subjects. Experiments are carried out on two public data sets to verify that anti-aliasing filter-based preprocessing can improve signal feature discrimination. The improved whale algorithm can find the optimal parameters of robust support matrix machine classification for individuals. This presented method can improve the recognition rate of dance motion image. Compared with other advanced methods, the proposed method requires less samples and computing resources, and it is suitable for the practical application of brain-computer interface.

Keywords: EEG signals classification, Dance motor imagery, Anti-aliasing filter, Whale parameter optimization, Two-dimensional empirical wavelet transform, Robust support matrix machine.

1. Introduction

Brain Computer Interface (BCI) technology aims to bypass the pathway between the brain and muscles by creating a signal transmission interface between the human brain and the machine [1]. It allows the user to control the external device directly through the brain, instead of using the traditional method of muscle movement. Therefore, BCI technology has a broad application prospect in patients with paralysis and confinement, as well as in extreme environments such as space. BCI technology involves signal processing, machine

⋆ Corresponding author

learning, cognitive neuroscience and other disciplines [2].

In so many BCI technologies, Electroencephalogram (EEG) is collected in the cerebral cortex in a non-invasive way, thus becoming a brain-computer interface technology suitable for ordinary people to participate in without ethical constraints and invasive brain operation [3]. In EEG based brain-computer interface technology, event-related potential, steady-state visual potential and sensory motor rhythm are the three main application methods. Here, the perceptual Motor rhythm is induced by Motor Imagery BCI (MI-BCI) [4]. MI-BCI mainly changes the energy of specific rhythm of EEG on the opposite side of the brain, and these energy changes are recorded by EEG, known as Event Related desynchronization phenomenon (ERD) [5]. Sensorimotor rhythm in the brain is widely distributed and controlled by different brain regions. However, due to the topological organization of motor neurons, EEG signals collected by the cerebral cortex are usually aliases of multiple motor sensing neurons, resulting in poor spatial resolution of the original EEG signal and affecting the pattern recognition results of the motor imagination EEG signal.

In order to improve the spatial resolution of ERD phenomenon in EEG, ensure pattern recognition accuracy of MI-BCI, commonly used feature extraction methods include spectral analysis, auto-regression, source reconstruction and Common Spatial Pattern (CSP) [6]. CSP brings spatial resolution advantage to ERD phenomenon, so it is widely used in the recognition of perceptual motor rhythm. Although CSP can distinguish signal maximization differences according to different tasks, the distinguishable characteristics often depend on the selection of frequency bands. Therefore, the frequency bands are divided into several sub-band Filter Bank CSPS (FB-CSP) to improve the recognition performance [7].

Researchers have successively proposed a large number of improved algorithms for CSP, including the CSP-based spatio-temporal filtering, the co-sparse spectral space mode, the regularization CSP and the regularization CSP-based probability model. All these methods achieve better results on the basis of traditional CSP characteristics. It is difficult to select the optimal frequency band because of the great difference of perception-motor rhythm of different objects. Zhang et al. [8] introduced sparse Bayesian learning method on the basis of CSP, and the selected frequency band could improve the classification performance. A large number of relevant studies have shown that CSP relies more on the frequency band range of energy changes generated by motion imagination in the process of feature extraction, so it is necessary to further study the frequency band range of CSP filtering to ensure better distinguishable features extracted by CSP.

After feature extraction, pattern recognition is usually accomplished by classifier. In early pattern recognition, mainstream shallow classifiers such as linear discriminant analysis or support vector machine were directly adopted [9]. In recent years, the wide application of deep learning in small sample classification has led to more applications of deep learning in pattern recognition of motor imagination EEG signals. Gao et al. [10] adopted deep self-coding network to reduce the dimensionality of time series of high-dimensional EEG signals, achieving better recognition effect. After introducing the Convolutional Neural Network (CNN) structure, Ahmed et al. [11] still carried out convolutional operations in the time domain and the space, respectively, to form the combined features and complete the classification. Apicella et al. [12] regarded the time domain of signals as different time segments, carried out convolution respectively, simulated FB-CSP by

neural network model, and obtained the current optimal effect on the brain-computer interface competition data set. On this basis, the further CNN classification structure and 3 Dimension CNN (3DCNN) classification structure have both achieved performance improvement on motion imagination data sets. Recurrent Neural Network (RNN) has also made initial progress [13]. Researchers regard FB-CSP features as time series and use RNN to identify feature sequences to achieve better results on different data sets.

Although the deep learning architecture represented by CNN can directly complete the recognition of motor imagination on the EEG signal, without the traditional feature extraction process. However, the training process of deep learning requires the support of a large number of samples and computing resources, so it is not applicable to the field of BCI where it is difficult to obtain a large number of EEG samples. In addition, the application of BCI usually requires real-time and free environment, which cannot match the fixed environment of a large number of computing resources [14]. Therefore, scholars began to use machine learning to process the whole multi-dimensional EEG matrix, and Support Matrix Machine (SMM) [15] and Robust SMM (RSMM) [16] are successful in recognizing small samples of EEG. This kind of algorithm adopts the idea of Support Vector Machine (SVM) to directly process the multidimensional EEG matrix, and regards the EEG as the superposition of real EEG and noise signals. In the process of iterative optimization, the original EEG signals are corrected through the separated noise signals, so as to improve the classification accuracy of EEG signals.

However, the parameters of RSMM classifier have a great influence on the pattern recognition results, and the parameters of different subjects are different. Thus, the anti-aliasing filter based on whale parameter optimization (A^{2}FWPO) method has been proposed in this paper for feature extraction and recognition of dance motor imagery EEG. In this method, anti-aliasing filter is used to obtain the deep-band features, and the filtered signals are extracted by two-dimensional empirical wavelet transform. RSMM completes the feature recognition. In the process of recognition, the improved whale algorithm is used to find the optimal RSMM parameters for different subjects, so that the EEG classification accuracy of each subject can be achieved.

The organizational structure of this article is as follows. Section 2 gives related works for this paper. In section 3, we detailed show the proposed method. Experiments and analysis are given in section 4. There is a conclusion in section 5.

2. Related Works

Brain-computer interface is a new type of information transmission channel between the brain and external electronic devices, which does not rely on muscle tissue and peripheral nerves. EEG has become one of the most effective data sources for decoding the cognitive activity of the brain due to its high temporal resolution, good portability and non-invasive nature. EEG motor imagination brain-computer interface belongs to the category of spontaneous brain-computer interface, whose purpose is to accurately identify the user's intention of body movement, which commonly includes the imagination of left hand, right hand, feet and tongue movement [17], it is of great significance for medical rehabilitation, leisure and entertainment and other fields.

The traditional research methods of motor imaging EEG recognition task first need to preprocess EEG signals, then select appropriate methods to extract EEG features under

different cognitive states and select the most recognizable feature subset, and finally complete the recognition of motor imaging EEG signals through machine learning method. Through in-depth analysis of the manifestations and mechanisms of EEG features, we can see that the control of limb movement is controlled by the cross movement consciousness of contralateral brain region during the process of right-right movement imagination, which makes EEG present typical neurophysiological features. The mu rhythm and beta band amplitude of the corresponding EEG region on the opposite side decrease (event-related desynchronization (ERD), while the mu rhythm and beta band amplitude of the corresponding EEG region on the same side increase (event-related synchronization (ERS)). Therefore, the presence of motor awareness on the left or right side of the body can be judged based on the above ERD and ERS phenomena. However, there is no significant difference in ERD/ERS phenomenon and no clear distribution of corresponding EEG band in the motion imaging EEG of the body under different motion modes (especially unilateral body motion only), and it has nonlinear and non-stationary transient characteristics. Therefore, EEG feature extraction and unilateral motion intention recognition are relatively difficult to achieve under different motion modes. At present, there are few researches in this field at home and abroad.

Based on linear discriminant analysis of EEG, Xiao et al. [18] realized the intention recognition of hand stretching in patients with stroke paralysis. Wang et al. [19] identified the grasping movement imagination of stroke patients based on power spectrum analysis and brain topographic map information. The above methods are based on traditional analysis methods to achieve motion intention recognition under a single hand movement. In order to further accurately depict and effectively classify EEG motion image features under different motion modes, further research is needed to quantitatively describe EEG transient nonlinear features. Lin et al. [20] obtained an average recognition accuracy of 92.8% on the BCI Competition III IVa dataset by using the high-order statistical features extracted from the wavelet packet decomposition sub-band and multi-scale principal component analysis (MSPCA) denoising method. Baig et al. firstly used the Common Spatial Pattern (CSP) algorithm to extract the feature sets under the left- and right-handed motion imagination state, and then used the differential evolution optimization algorithm to extract the optimal feature subsets of each subject. Finally, it was sent into the Support Vector Machine (SVM) to build the classification model. The average classification accuracy of BCICompetition III dataset IVa was more than 95%. Faced with complex and unstructured data, traditional machine learning and statistical methods often require a certain feature engineering ability to extract more effective features or select more appropriate model parameters, while deep learning can train more abstract and effective features to complete end-to-end learning tasks.

Lopes et al. [21] used Short-Time Fourier Transform (STFT) to extract the time-frequency information of and rhythm in each channel, and combined them into 2D information as the input of the network. The Network was a deep network formed by the combination of Convolutional Neural Network (CNN) and Stacked Auto-Encoder (SAE), and classified the features extracted by CNN through SAE. The Kappa value of the proposed method on the dataset BCI Competition V dataset 2b was 0.547. Ma et al. [22] proposed a novel convolutional neural network for pattern recognition of motion imagery EEG. In this network, two convolution layers were set to extract the spatial and temporal features of signal sequences respectively.

3. Proposed Method

3.1. Feature Extraction Strategy

Task recognition of dance motor imagery EEG consists of two parts: signal feature extraction and pattern recognition. In this paper, anti-aliasing filter is used to extract the frequency-domain features of EEG signals, and two-dimensional empirical wavelet transform is used to extract the spatial features, which are composed of frequency-spatial features for pattern recognition of dance motion imagery tasks. In pattern recognition, the matrix form of EEG frequency domain-spatial characteristics is retained, and RSMM is used to complete the classification of motion imagination tasks. Due to the great difference of EEG in different individuals, the parameters used by RSMM in actual classification are different. Therefore, whale algorithm is adopted to automatically find the optimal classification parameters according to the characteristics of different individual signals, so as to achieve the highest recognition rate of the motion imagination EEG patterns of each individual.

The main principle of motion image pattern recognition is the event-related desynchronization phenomenon (ERD) in the process of imagination, which is reflected as the energy suppression of μ rhythm (8-12Hz) and β rhythm (18-24Hz) of EEG signal. In order to recognize the pattern of energy suppression, EEG pretreatment is needed. Common EEG acquisition devices generally collect signals between 0.1 and 100 Hz, but the signals generated by the discharge of neurons in the cerebral cortex are concentrated between 4 and 40 Hz. Therefore, the primary task of pre-processing is to keep the EEG frequency band between 4 and 40 Hz through band-pass filter. However, the detailed energy suppression caused by ERD cannot be obtained in a wide band, so the pattern recognition results are not ideal [23].

If no aliasing occurs in the sampled signal, down-conversion is performed to convert the sampled signal into base-band signal, and each signal in the multi-band communication signal is separated one by one. If two signals in the same frequency domain are aliased after sampling, the following analysis is carried out.

The two signals with aliasing after sampling are defined as $R_0(f)$ and $R_1(f)$. The delay difference between the first and second sample streams is T. The spectrum of the two signals after the first sampling flow is $R_A(f)$, and the spectrum after the second sampling flow is $R_B(f)$. $R_A(f)$ and $R_B(f)$ satisfy the relationship:

$$\begin{cases} R_A(f) = R_{0A}(f) + R_{1A}(f) \\ R_B(f) = R_{0B}(f) + R_{1B}(f) \\ R_B(f) = R_{0A}(f)e^a + R_{1A}(f)e^b \end{cases} \tag{1}$$

Assuming that the communication number of the RF band to be sampled is $R(f)$ and its bandwidth is B. The sampling frequency f_s is adopted, which is $f_s = 2B$. Where $a = e^{-j2\pi\Delta T f_s n_0}$, $b = e^{-j2\pi\Delta T}$. $((n+1)/2)f_s < |f| < ((n+1)/2)f_s$.

The two digital signals obtained by the second order sampling module are aliased by an anti-aliasing filter. Anti-aliasing filters $S_A(f)$ and $S_B(f)$ are designed and applied to channel A and channel B respectively. The recovered signal spectrum then becomes:

$$R(f) = B \times [S_A(f) \cdot R_A(f) + S_B(f) \cdot R_B(f)] \tag{2}$$

By splitting the normal spectrum and secondary spectrum of the signal, Equation (2) takes the transformation as:

$$R(f) = B \times [S_A(f) \cdot (R_{A+}(f) + R_{A-}(f)) + S_B(f) \cdot (R_{B+}(f) + R_{B-}(f))] \quad (3)$$

For each channel, there are signals from frequency positions a and b, so Formula (2) is further decomposed as:

$$\begin{aligned} R(f) =& B \times [S_A(f) \cdot (R_{0A+}(f) + R_{1A+}(f) + (R_{0A-}(R_{1A+}(f)) \\ &+ S_B(f) \cdot (R_{0B+}(f) + R_{1B+}(f) + R_{0B-}(f) + R_{1B-}(f)] \end{aligned} \quad (4)$$

Filters $S_A(f)$ and $S_B^0(f)$ are designed to restore $R_0(f)$ and eliminate $R_1(f)$. Therefore, the filters $S_A(f)$ and $S_B^0(f)$ should satisfy the follows:

$$B \times [S_A(f) \cdot R_{0A+}(f) + S_B^0(f) \cdot R_{0B+}(f)] = C \cdot R_{0A+}(f - 2aB) \quad (5)$$

$$B \times [S_A(f) \cdot R_{0A-}(f) + S_B^0(f) \cdot R_{0B-}(f)] = C \cdot R_{0A-}(f - 2aB) \quad (6)$$

$$B \times [S_A(f) \cdot R_{1A+}(f) + S_B^0(f) \cdot R_{1B+}(f)] = 0 \quad (7)$$

$$B \times [S_A(f) \cdot R_{1A-}(f) + S_B^0(f) \cdot R_{1B-}(f)] = 0 \quad (8)$$

Where C is the amplitude gain of the signal. Here, $S_A(f)$ is chosen as the simplest form, i.e.,

$$S_A(f) = \begin{cases} 1/B & |f| < B \\ 0 & otherwise \end{cases} \quad (9)$$

Therefore, by solving equations (7) and (8), $S_B^0(f)$ can be obtained as follows.

$$S_B^0(f) = \begin{cases} -\dfrac{\beta^{-b}}{B} & -B < f < 0 \\ -\dfrac{\beta^{b}}{B} & 0 < f < B \\ 0 & otherwise \end{cases} \quad (10)$$

Equations (8)-(10) are expressions of filters in the frequency domain. Their impulse response can be obtained through equations (8)-(10), and the filter impulse response can be written as:

$$S_A(t) = \int_{f_t}^{f_h} S_A(f) e^{j2\pi ft} dt \tag{11}$$

$$S_B^0(t) = \int_{f_t}^{f_h} S_B^0(f) e^{j2\pi ft} dt \tag{12}$$

$$S_B^1(t) = \int_{f_t}^{f_h} S_B^1(f) e^{j2\pi ft} dt \tag{13}$$

f_t and f_h are the lowest and highest frequencies of the anti-aliasing filter, respectively. By sampling the sampled signal with $f_s = 2B$, the sampled value can be used as the parameter of anti-aliasing filter. When the signal position index changes, the same S_A can still be used. However, for S_B, when the position index changes, the filter parameters need to be adjusted according to the position index.

Due to the anti-aliasing filter, the restored signal has a certain amplitude difference from the original signal. By substituting equations (8) and (9) into equation (6), the expression of amplitude gain can be obtained, as shown in Equation (14).

$$|C| = |1 - \beta^{\pm(b-a)}| = \sqrt{2 \cdot 1 - cos[2\pi T_\Delta f_s |b-a|]} \tag{14}$$

As can be seen from Equation (14), better gain effect can be obtained by adjusting T_Δ value in real time according to the position of a and b.

3.2. Constraint Condition

The sampling frequency of the second-order band-pass sampling module should follow the following formula.

$$\begin{cases} n_k \cdot f_s - f_s/2 < f_{lk} < f_{uk} < n_k \cdot f_s + f_s/2 \\ |f_{Ncb} - f_{Nca}| \geq \dfrac{B_a + B_b}{2} \end{cases} \tag{15}$$

In $n_k \cdot f_s - f_s/2 < f_{lk} < f_{uk} < n_k \cdot f_s + f_s/2$, n_k is the position index of the $k-th$ signal in the multi-band RF band communication signal. f_s is the sampling frequency. f_{lk} and f_{uk} are the lowest and highest frequencies with communication number k, respectively. This formula limits aliasing of sampled signal images. At the same time, the multi-band communication number should also satisfy $|f_{Ncb} - f_{Nca}| \geq \frac{B_a+B_b}{2}$. This formula can be used to avoid overlapping of more than two signals after sampling. B_a and B_b are the processing bandwidths of the two sampled RF bands. f_{Ncb} and f_{Nca} are the signal center frequencies of the sampled two-way tape signal in the first Nyquist region.

In fact, due to the nonlinear and non-stationary characteristics of EEG signals, the feedback of different subjects and the same subjects to motor imagination in different

stages of motor imagination has a floating range in different sub-bands [24]. Some subjects may have rhythms in the 6-11Hz range, while others may have rhythms in the 20-28Hz range. The floating range of rhythm and rhythm in the sub-band cannot be dealt with by simply dividing multiple sub-bands with the range of 4Hz. This paper proposes that anti-aliasing filter can be divided into different sub-bands according to different overlapping range combinations.

3.3. Two-Dimensional Empirical Wavelet Transform

Two-dimensional empirical wavelet transform is an improvement on the classical two-dimensional Littlewood Paley wavelet transform. Its filter bank has a ring support in Fourier domain, and the inner and outer radii of the support are fixed on the binary decomposition plane of Fourier domain, namely the scale factor [25]. Here, empirical analysis method is applied to detect each ring supported by the ring. The detection is carried out in Fourier's pseudo-polar plane, so the boundary can be represented by the frequency modulus $|\omega|$. In order to solve the construction problem of Fourier transform of pseudo-poles, references [26,27] put forward some methods, and provided an operator $F_p(f)(\theta, |\omega|)$ to construct it. In the Fourier support, the one-dimensional Fourier spectrum exists in each Angle θ. However, under tensor transformation, if Fourier boundary detection is performed separately for each Angle θ, there will be some discontinuities in the output spectrum. In order to avoid this influence, two-dimensional empirical wavelet transform adopts the idea of tensor transformation to calculate the average spectrum, namely,

$$\tilde{F}(|\omega|) = \frac{1}{N_\theta} \sum_{i=0}^{N_\theta - 1} F_p(f)(\theta_i, |\omega|) \tag{16}$$

Where, N_θ is the number of discrete angles. Then, the spectrum $\tilde{F}(|\omega|)$ is boundary detected, and the set ω^n. This set is used to construct a set of two-dimensional experiential Littlewood Paley wavelets.

$$B^{ELP} = \varphi_1(X), \phi_n(X)_{n=1}^{N-1} \tag{17}$$

Where, $\phi_n(X)$ is the empirical wavelet function. $\varphi_1(X)$ is the empirical scale function. B^{ELP} is established for a set of two-dimensional empirical wavelets. This definition is a direct extension of one-dimensional empirical wavelet. Since the extension of the ring over $\omega^{N-1} \leq |\omega| \leq \omega^N$ is to preserve the "Angle" of the Fourier domain, it is defined as shown in equations (18)-(20), except for the last ring.

$$F_2(\varphi_1)(\omega) = \begin{cases} 1 \quad |\omega| \leq (1-\gamma)\omega^1 \cdot A \\ if(1-\gamma)\omega^1 \leq \omega \leq (1+\gamma)\omega^1 \\ 0 \quad otherwise \end{cases} \tag{18}$$

If $n \neq N-1$, then

$$F_2(\varphi_n)(\omega) = \begin{cases} 1 \quad if(1-\gamma)\omega^n \le \omega \le (1+\gamma)\omega^{n+1} \cdot A \\ if(1-\gamma)\omega^{n+1} \le \omega \le (1+\gamma)\omega^{n+1} \cdot B \\ if(1-\gamma)\omega^n \le \omega \le (1+\gamma)\omega^n \\ 0 \quad otherwise \end{cases} \tag{19}$$

$$F_2(\varphi_{n-1})(\omega) = \begin{cases} 1 \quad if(1+\gamma)\omega^{N-1} \le |\omega| \cdot B \\ if(1-\gamma)\omega^{N-1} \le \omega \le (1+\gamma)\omega^{N-1} \\ 0 \quad otherwise \end{cases} \tag{20}$$

Here, $A = cos[\frac{\pi}{2}\beta(\frac{1}{2\gamma\omega^1}(|\omega| - (1-\gamma)\omega^1))]$ and $B = sin[\frac{\pi}{2}\beta(\frac{1}{2\gamma\omega^n}(|\omega| - (1-\gamma)\omega^n))]$. The detail coefficient of the two-dimensional empirical wavelet transform of signal f is defined as:

$$W_f^{ELP}(n, X) = F_2^*(F_2(f)\omega)\overline{F_2(\phi_n)(\omega)} \tag{21}$$

The approximate coefficient (conventionally expressed by $W_f^{ELP}(0, X)$) is:

$$W_f^{ELP}(0, X) = F_2^*(F_2(f)\omega)\overline{F_2(\phi_1)(\omega)} \tag{22}$$

Its inverse transformation is:

$$f(x) = F_2^*(F_2(W_f^{ELP})(0,\omega)F_2(\varphi_1(\omega)) + \sum_{n=1}^{N-1} F_2(W_f^{ELP})(n,\omega)F_2(\phi_n)(\omega)) \tag{23}$$

From the above analysis, the algorithm flow of 2D-EWT image processing can be obtained as **Algorithm 1**.

3.4. Robust Support Matrix Machine Pattern Recognition Method

After anti-aliasing filtering in frequency domain and two-dimensional empirical wavelet transform filtering in spatial domain, a stable frequency-spatial characteristic matrix can be generated. In the traditional machine learning model, the pattern recognition of frequency domain-spatial eigenmatrix usually needs to be transformed into vector form, such as linear discriminant analysis and support vector machine. The vector form does not retain the spatial geometric relationship of the original EEG signal, and the accuracy of pattern recognition is not high. The deep learning model is directly carried out on the frequency-spatial eigenmatrix. Due to the ”black box” property of convolutional neural network, accurate optimization strategy cannot be given. Experiments show that EEG recognition performance can be better if the model is not deeper, which is usually due to the nonlinear and non-stationary characteristics of EEG. Therefore, the classification of EEG frequency domain-spatial characteristic matrix should be completed by accurate and

Algorithm 1 2D-EWT process

Input: signal $f(x)$, filter number N.

1: Step 1. Calculate $F_p(f)(\theta, |\omega|)$ and find the average spectrum.

$$\tilde{f}(|\omega|) = \frac{1}{N} \sum_{i=0}^{N_\theta - 1} |F_p(f)(\theta_i, |\omega|)|$$

2: Step 2. The Fourier boundary is detected by Equations (18)-(20), and the spectral radius set and the corresponding filter banks are obtained.

$$B = \varphi_1(X), \phi_n(X)_{n=1}^{N-1}$$

3: Step 3. The original signal is filtered by equations (21) and (22), and the target signal f is obtained. **Output: B^{ELP} and $W_f^{ELP}(n, X)$**

stable optimization strategy on the basis of preserving the geometric characteristics of the matrix.

In this paper, robust support matrix machine (RSMM) is introduced to complete the identification of dance EEG frequence-spatial characteristic matrix. Suppose two categories of dance motor imagination training set are represented as $x_t, y_t{}_{t=1}^{T}$. Where, $X_t \in R^{d_1 \times d_2}$ represents the extracted feature of the $t-th$ signal sample. d_1 represents the frequency-spatial dimension. d_2 represents the time domain dimension. $y_t \in -1, 1$ represents the true label of the $t-th$ signal sample.

Pattern recognition for multiple categories of dance motion imagination can still be used in One versus All (OVA) way. RSMM regards the anti-aliasing filter two-dimensional empirical wavelet transform (AF-TDEWF) feature matrix as the sum of low-rank noiseless feature matrix $L_t \in R^{d_1 \times d_2}$ and noise feature matrix $S_t \in R^{d_1 \times d_2}$:

$$X_t = L_t + S_t \tag{24}$$

In the training process, the noiseless low-rank brain feature matrix is used to replace the original feature matrix to complete the pattern recognition problem of dance motion imagination. According to the maximum interval theory of SVM, RSMM regards the pattern recognition problem as the minimum maximum interval with regular term:

$$\underset{W,b}{Min} \sum_{t=1}^{T} 1 - y_t[tr(W^T L_t) + b]_+ + \lambda_1 ||W||_* + \sum_{t=1}^{T} (\lambda_2 ||L_t||_* + \lambda_3 ||L_t||_1) \tag{25}$$

Where, W and b represent the classification hyperplane and bias of the two categories of dance motion imagination. $\lambda_1 ||W||_*$ represents the regular term of hyperplane pair optimization. $\lambda_2 ||L_t||_*$ represents that the address noiseless eigenmatrix adopts kernel norm for the regular term of the optimization function. $\lambda_3 ||L_t||_1$ represents the regular term of the noise characteristic matrix against the optimization function, using the l_1-norm.

Since this optimization problem cannot be directly transformed into a vector, the optimization process of SVM cannot be adopted, and there are 4 variables and the joint minimization problem of kernel norm and norm, so the iterative optimization process with alternating optimization directions can only be adopted. In the RSMM solution process, the interval is rewritten as:

$$h(W, b, L_t) = 1 - y_t[tr(W^T L_t) + b]_+ \tag{26}$$

The hyperplane regular term is rewritten as $W = Z$, then we introduce augmented Lagrange multiplier V, $X_t \in R^{d_1 \times d_2}$, the augmented Lagrange function of Equation (25) can be given to solve the optimization problem with restrictive conditions:

$$\begin{aligned} h(W, Z, b, L_t, S_t, V, M_t) = & \sum_{t=1}^{T} h(W, b, L_t) + \lambda_1 ||Z||_* \\ & + tr[V^T(Z - W)] + \frac{\mu_1}{2}||Z - W||_F^2 \\ & + \sum_{t=1}^{T} \lambda_2 ||L_t||_* + \lambda_3 ||S_t||_1 \\ & + \sum_{t=1}^{T} tr[M_t^T(X_t - L_t - S_t)] \\ & + \sum_{t=1}^{T} \frac{\mu_2}{2}||X_t - L_t - S_t||_F^2 \end{aligned} \tag{27}$$

Where, μ_1 and μ_2 are the two penalty parameters of the augmented Lagrange multiplier respectively, and both are positive numbers. Given appropriate Lagrangian multipliers V, $X_t \in R^{d_1 \times d_2}$ and the corresponding penalty parameters μ_1 and μ_2 (large positive numbers), the Lagrangian multipliers are augmented to optimize Equation (27) by iterative optimization in alternating optimization directions, and the minimization result of Equation (27) is the same as that of Equation (25) with constraints.

3.5. Parameter Optimization

In the minimization function constructed by RSMM, there are three regular term parameters λ_1, λ_2, λ_3, which are usually set as $\lambda_1 = 1$, $\lambda_2 = 0.1$, $\lambda_3 = 0.01$ by default in dance motion imaginary pattern recognition. In fact, due to the sensitivity of EEG electrodes, the EEG stability of different subjects is different, and the noise introduced in the acquisition process is also different. Therefore, it is not reasonable to adopt the same regularization parameters to correct and optimize the process for all test subjects, and different subjects have regularization parameters more suitable for EEG morphology. Therefore, the modified whale algorithm is introduced into the parameter optimization of RSMM to provide more scientific and reasonable regularization parameters for EEG of different test subjects.

Whale Optimization algorithm (WOA) is an algorithm proposed by Mirjalili et al to simulate humpback whale bubble net feeding [28]. This algorithm is essentially a meta-heuristic algorithm based on swarm intelligence simulation.

A. Surrounding the prey WOA considers prey location as the optimal target or approximate optimal solution, and individuals in other populations update their positions based on this process. The mathematical model of this process can be expressed by the following formula:

$$\begin{cases} D = |C \times X^*(t) - X(t)| \\ X(t+1) = X^*(t) - A \cdot D \\ A = 2ar - a \\ C = 2r \end{cases} \tag{28}$$

Where t represents the number of iterations. A and C represent the coefficient vector. X^* is the current best whale position. X is the current whale position. a decreases linearly from 2 to 0 during iteration. r represents the random number in the interval [0-1].

B. Bubble net attack mode Bubble net attack can be divided into two strategies: shrink surround and spiral update position.

1)shrink surround.

This is achieved by the a value in the formula. a is reduced from 2 to 0 during the iteration, and A is a random number in the interval ($-a$,a), that is, a is a random value in (-2, 2). When A is set from -1 to 1, the whale's new position can be defined as anywhere between the original position and the prey position.

2)spiral update position.

Firstly, the distance between the whale and the prey position is calculated, and then the spiral equation is established between the two positions to simulate the spiral motion of the whale:

$$\begin{cases} X(t+1) = D \cdot e^{bl} \cdot cos(2\pi l) + X^*(t) \\ D = |X^*(t) - X(t)| \end{cases} \tag{29}$$

Where D is the distance between the whale and its prey. b represents spiral shape constant. l is the random number in the interval [-1,1].

While shrinking to encircle prey, the whale hunts prey in a spiral orbit. In order to simulate this simultaneous behavior, suppose that there is a probability of 0.5 to make a choice between shrinking to encircle the prey and the spiral model to update the whale position, then the mathematical model is as follows:

$$X(t+1) = \begin{cases} X^*(t) - A \cdot D & p < 0.5 \\ D \cdot e^{bl} \cdot cos(2\pi l) + X^*(t) & p \geq 0.5 \end{cases} \tag{30}$$

C. Hunt for prey Whales look for prey based on each other's positions. When $|A| > 1$, the whale position is updated by random selection. The mathematical model is as follows:

$$\begin{cases} X(t+1) = Xrand(t) - A \cdot D \\ D = |C \cdot Xrand(t) - X(t)| \end{cases} \tag{31}$$

Where $Xrand(t)$ represents the location of random whales.

3.6. Process of Proposed Method

Finally, the feature matrix is first extracted from the dance motion imaging EEG signal, the improved whale algorithm is used to obtain the optimal parameters for each test object, and the RSMM of the optimal parameters is used for pattern recognition of the extracted feature matrix. In the proposed method, the three parameters λ_1, λ_2, λ_3 of RSMM initialization vary greatly according to the EEG of different individuals. Since there are only 4 overlapping ranges, the suitable overlapping ranges of EEG signals from different individuals can be determined by pre-experiment. However, the value range of the three parameters of RSMM is:

$$1 \leq \lambda_1 \leq 10, 0.11 \leq \lambda_2 \leq 1, 0.01 \leq \lambda_3 \leq 0.1 \tag{32}$$

Therefore, whale algorithm is used to select appropriate parameters for EEG signals of different subjects. The negative recognition rate of dance motion image is taken as the fitness function of whale algorithm:

$$fitness(i) = RSMM(AF - TDEW, L, \lambda_1, \lambda_2, \lambda_3) \tag{33}$$

Where, i is the number of iterations. $fitness(i)$ is the fitness function. L is the dance motor imagination task tag.

By minimizing the fitness function of the whale algorithm, the parameters with the highest recognition rate of each individual EEG signal can be found, and the optimal recognition parameters of individual dynamic adjustment can be formed. The specific process of the method in this paper is shown in Figure 1.

The time complexity of the proposed method consists of three parts: feature extraction, RSMM classifier iterating, WOA to find the optimal parameters, and form a robust pattern recognition method for supporting matrix machine. Suppose that the training samples are n EEG matrices of size $d_1 \times d_2$. d_1 is the number of electrodes. d_2 is the number of signal sampling points. AF-TDEW generates f frequency bands, and the signal matrix of each band needs to calculate feature decomposition. The time complexity is as follows:

$$O(min(fd_1^2 d_2, fd_1 d_2^2)) \tag{34}$$

In the RSMM classifier training iteration process, eigenvalue decomposition of Z and L should also be calculated, and the time complexity is respectively:

$$O(min(d_1^2 d_2, d_1 d_2^2)) \tag{35}$$

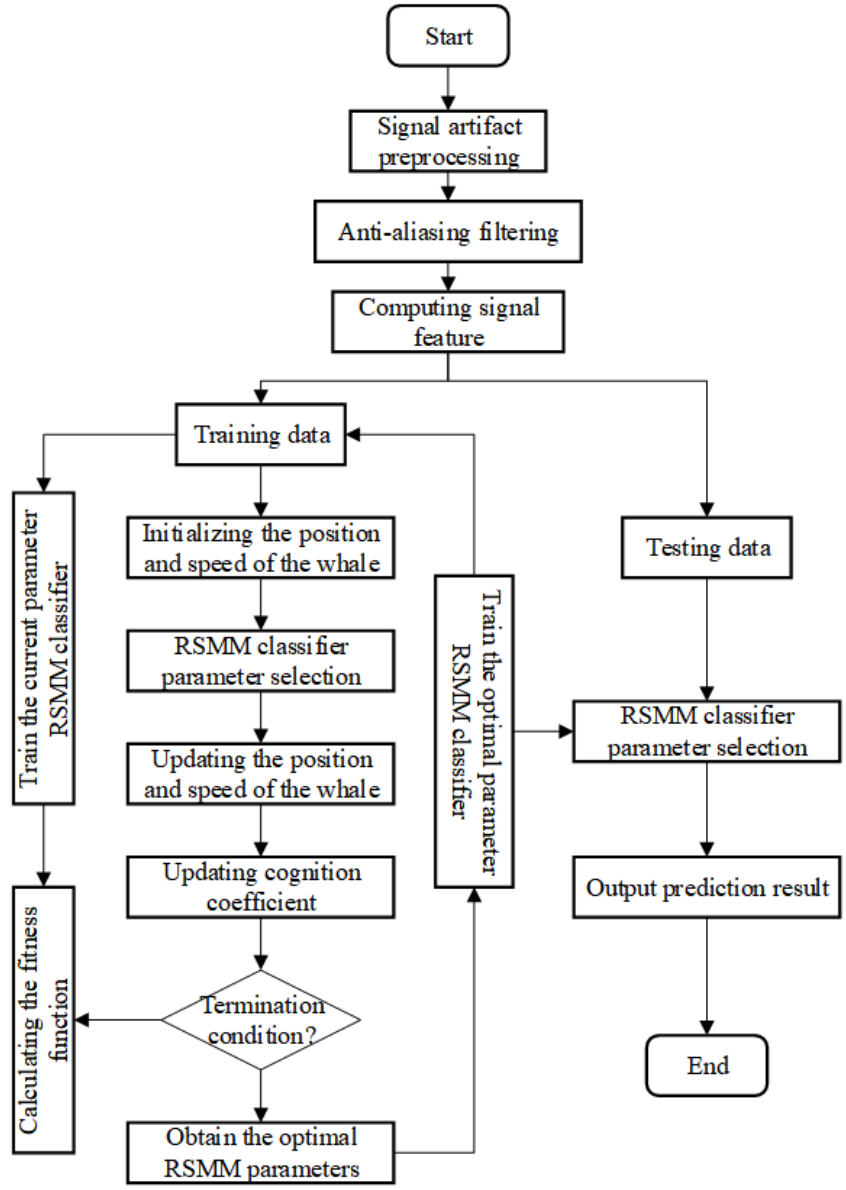

Fig. 1. The flow chart of proposed method in this paper

$$O(min(nd_1^2d_2, nd_1d_2^2)) \tag{36}$$

In addition, RSMM also needs to solve the weight W through quadratic programming, and the time complexity is $O(n^2d_1d_2)$. AF-TDEW only modifies c_1 and c_2 parameters on the basis of WOA. Theoretically, the time complexity is the same as WOA, but the iterative convergence process of parameters reduces the number of iterations for obtaining the optimal solution of AF-TDEW. Because the number of EEG electrodes and the number of signal sampling points are usually small, $d_1 \ll d_2 < 1000$. The value ranges of the three parameters optimized by AF-TDEW are all small. Therefore, assuming that the number of iterations of RSMM is K_1, the iteration number of AF-TDEW is K_2, and the number of whale population is m, the time complexity of the proposed method is:

$$O(K_1(n^2d_1d_2) + mK_2 \tag{37}$$

4. Experiments and Analysis

4.1. Data Set and Preprocessing

In this paper, BCI Competition II dataset III exercise imagination dataset is selected, which records 300 random left and right hand exercise imagination experiments of a normal female subject. Some samples are shown in figure 2. 150 experiments are selected in a random way as the training set and the remaining 150 experiments as the test set [29]. The training set consists of 75 left hand visuals and 75 right hand visuals. During the whole collection process, the EEG signal is recorded at the sampling frequency of 128 Hz, and the band pass filtering is performed at 0.5-30Hz. The time flow of each experiment in the process of data acquisition is shown in Figure 3.

The duration of each experiment is 9s, and there will be 2s preparation time after the beginning of the experiment. At the beginning of the third second, there will be a short sound indicating that the subjects are about to perform the dance motion imagination task, and at the same time, the screen shows a cross "+" lasting 1s. From the fourth second, an arrow will appear on the screen, and the subjects drags the feedback bar to move in the direction indicated by the arrow through motion imagination. And it holds until the end of the ninth second.

There are regular electrical changes in the motor sensory cortex of the brain when people imagine body movements. When the subjects imagined unilateral limb movement, the intensity of μ rhythm (8-12Hz) in the contralateral cortex decreased, while the intensity of β rhythm (12-25Hz) in the ipsilateral cortex increased. These are called Event Related Desynchronization (ERD) and Event Related Synchronization (ERS) phenomena. These two phenomena are important basis for distinguishing different types of EEG signals, among which time-frequency domain analysis is one of the most efficient analysis methods.

Fig. 2. Samples in dataset

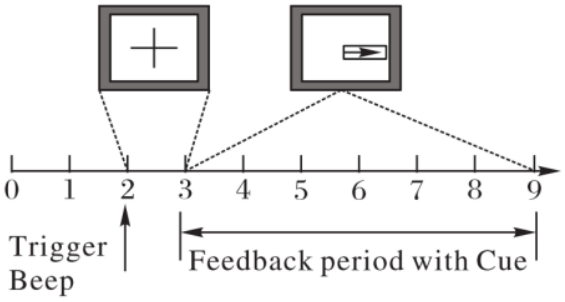

Fig. 3. Time sequence diagram of single dance motion imagination task

4.2. Experimental Environment and Implementation

In the process of dance motor imagination paradigm, EEG extraction of dance motor imagination is concentrated in the time range of 3-6s, and 3.5-6s time period is selected for pattern recognition of dance motor imagination when verifying the method. We split the data set in two sets: Dataset 2a and Dataset 2b. Dataset 2a data sets have 4 labels. OVA is used for pattern recognition to compare one category with the other three categories. Dataset 2b data sets have 2 labels and are completed using a common binary classification.

Parameters are set as follows: $d_1 = 25$, $d_2 = 630$. In Dataset 2a $n = 288$, in Dataset 2b $n = 400$. Parameters of WOA are initialized as $c_1 = 2$, $c_2 = 0$, $w = 1$, and the maximum population number $m = 50$. The iteration number of RSMM is set to $K_2 = 500$. The iteration number of RSMM is set to $K_1 = 10$ and $K_2 = 50$ in Dataset 2a and Dataset 2b respectively.

The simulation platform of the experiment is Matlab R2017a with Intel i7-9700 CPU, 64 GB memory and 64-bit Windows 11 operating system. EEG data sets from the BCI Competition IV are in GDF format and accessed through the Biosig toolbox (http://biosig.sourceforge.net).

4.3. Experimental Results of Feature Extraction

In order to verify the extraction results of AF-TDEW features, session 1 and session 4 of S_6 on Dataset2b data set are taken as examples. Three different overlapping ranges of anti-aliasing filter A^{2}F=0,1,2,3,4 are set, and AF-TDEW features are extracted after filter preprocessing. Table 1 shows the best and second-best features of AF-TDEW in five overlapping ranges.

Table 1. The proportion of the best and second-best features of AF-TDEW in five overlapping ranges/%

A^{2}F	Best	Second-best
0	88.7	89.1
1	89.3	90.2
2	85.6	87.8
3	82.9	83.3
4	78.5	79.4

As can be seen from Table 1, anti-aliasing filtering can affect the features of two-dimensional empirical wavelet transform, especially the best features and second-best features. According to the calculation process of two-dimensional empirical wavelet transform feature, the feature needs to find the feature with the maximum distinction between the two categories, so as to ensure that the feature can be used to identify different motion imagination modes to the maximum extent. According to the best features and second-best features displayed by the two class training sets and test sets, the best features and second-best features extracted by two-dimensional empirical wavelet transform can be separated according to the class after anti-aliasing filtering. The separation occurs in both the training set and the test set. The smaller the overlap range is, the more detailed band

energy the filter banks can obtain. Therefore, compared with A^2F=0,2,3,4, A^2F=1 can distinguish different categories of two-dimensional empirical wavelet transform features more greatly.

In dance motion image pattern recognition, SVM, RSMM and AF-TDEW+RSMM are used respectively to compare the extracted features. SVM uses polynomial kernel function parameters $C = 2.5$, $g = 0.02$. RSMM parameter: $\lambda_1 = 1$, $\lambda_2 = 0.1$, $\lambda_3 = 0.01$.

Table 2 and Table 3 show the results of dance motion image pattern recognition of AF-TDEW features in different classifiers.

Table 2. When A^2F=1, recognition accuracy with different classifiers on Dataset 2a/%

Subject	SVM	RSMM	AF-TDEW+RSMM
S1	83.75	84.44	85.11
S2	54.58	49.72	55.99
S3	80.28	86.18	86.49
S4	59.44	53.54	61.27
S5	41.04	41.96	42.92
S6	50.76	51.86	53.24
S7	84.79	85.49	87.92
S8	72.97	71.25	73.38
S9	71.60	69.39	72.84

Table 3. When A^2F=1, recognition accuracy with different classifiers on Dataset 2b/%

Subject	SVM	RSMM	AF-TDEW+RSMM
S1	64.55	69.56	73.92
S2	57.90	58.21	60.32
S3	54.55	57.36	59.63
S4	91.42	94.23	96.43
S5	76.42	77.51	76.65
S6	77.36	81.67	83.92
S7	75.80	76.95	77.92
S8	81.12	84.86	87.67
S9	75.81	76.74	78.92

It can be seen from Table 2 and Table 3 that, on the two dance motion imagination data sets, AF-TDEW+RSMM has higher pattern recognition accuracy.

4.4. Pattern Recognition Result

In order to verify the role of WOA in RSMM parameter optimization, Genetic Algorithm (GA) [30], Quantum Immune GA (QIGA) [31] and PSO are adopted to conduct comparison experiments. The comparison of the four algorithms is carried out on the basis

A^{2}F=1, and tables 4,5 show the pattern recognition results of RSMM based on the four algorithms.

Table 4. Recognition accuracy by different parameter optimization methods on Dataset 2a/%

Subject	GA	QIGA	PSO	WOA
S1	80.2	81.7	84.1	85.6
S2	54.8	56.4	57.3	58.9
S3	84.7	86.5	87.3	89.6
S4	55.6	57.9	59.1	60.2
S5	48.3	52.7	54.2	55.7
S6	54.5	56.3	58.4	59.1
S7	87.4	89.6	91.1	92.3
S8	74.7	76.9	78.4	80.5
S9	68.7	70.6	72.5	73.5

Table 5. Recognition accuracy by different parameter optimization methods on Dataset 2b/%

Subject	GA	QIGA	PSO	WOA
S1	65.4	67.2	68.7	69.2
S2	52.8	54.6	56.4	58.7
S3	56.7	57.1	58.2	59.4
S4	92.1	94.5	96.5	98.8
S5	79.6	81.1	82.1	83.6
S6	77.5	78.9	80.7	82.4
S7	78.3	80.2	81.6	82.9
S8	82.9	84.3	86.2	88.3
S9	76.7	77.1	78.5	79.6

As can be seen from Table 4 and 5, the overall improved WOA better optimizes the pattern recognition results of RSMM. According to the classification accuracy of 9 subjects in Dataset 2a and Dataset 2b, WOA is superior to GA, QIGA, PSO in parameter optimization of RSMM classifier.

In addition, in terms of the provided experimental simulation platform parameters, Table 6 shows the comparison of the running time of the four algorithms on the two data sets. As can be seen from the table 6, WOA and QIGA need more computing steps than PSO and GA, thus generating greater time complexity. Compared with QIGA, WOA not only achieves higher classification accuracy, but also requires more iterations and corresponding optimization time.

Combined with the above experimental results, using AF-TDEW+RSMM pattern recognition method, the optimal recognition results on the two data sets are presented

Table 6. Running time comparison with four algorithms on two data sets/s

Method	Dataset 2a	Dataset 2b
GA	498.97	2497.87
QIGA	503.78	2519.39
PSO	280.58	1497.49
WOA	519.34	2769.60

in Table 7 and Table 8 respectively. The iteration number of RSMM in Dataset 2a and Dataset 2b is set to 10 and 50 respectively.

Table 7. The optimal recognition results of the proposed method on Dataset 2a

Subject	Training time/s	Test time/s	Best accuracy/%
S1	98.67	17.68	86.53
S2	242.70	40.63	54.33
S3	80.24	14.04	87.32
S4	203.40	37.21	60.37
S5	201.03	35.18	48.26
S6	95.57	16.07	56.19
S7	198.84	35.30	89.96
S8	195.31	32.86	74.42
S9	105.87	17.01	70.67

Table 8. The optimal recognition results of the proposed method on Dataset 2b

Subject	Training time/s	Test time/s	Best accuracy/%
S1	78.20	44.11	70.74
S2	87.31	51.71	57.61
S3	83.71	51.34	57.62
S4	11.77	5.21	96.86
S5	164.25	72.38	83.24
S6	63.92	39.74	79.49
S7	142.84	64.73	76.99
S8	11.61	4.99	88.24
S9	75.38	41.14	78.86

It can be seen from the statistical data in Table 7 and Table 8 that the classification accuracy of Dataset 2a and Dataset 2b is greatly improved. When the sample size is 288 (Dataset 2a) and 320(Dataset 2b), the ratio of training time to testing time is about 6 times. The training time and test time of the proposed method are relatively stable, which is suitable for the application scenario of brain-computer interface. The influence time is only affected by different overlap parameters.

In order to compare the proposed method, the optimal recognition results of the proposed method are compared with other state-of-the-art methods including MSCNN [32], CNN-LSTM [33], DANN [34], and LFFN [35]. Table 9 shows the optimal recognition accuracy of each method. Table 10 shows the p-value values of the new method in this paper and other methods.

Table 9. The optimal recognition results of each method/%

Method	Dataset 2a	Dataset 2b
MSCNN	66.58	74.79
CNN-LSTM	68.38	77.23
DANN	68.69	77.63
LFFN	69.84	78.21
Proposed	75.49	79.87

Table 10. The p-value results of each method

Method	Dataset 2a	Dataset 2b
MSCNN	0.862	0.986
CNN-LSTM	0.778	0.845
DANN	0.729	0.763
LFFN	0.684	0.541
Proposed	p¡0.01	p¡0.01

As can be seen from Table 9 and Table 10, the pattern recognition accuracy of this method is higher than that of other methods on Dataset 2a and Dataset 2b. In fact, deep learning methods require a large number of samples and training calculations, and are not applicable in the field of brain-computer interfaces. The proposed method requires only a small amount of samples and computation, and can obtain the pattern recognition results of motion imagination similar to deep learning, which has wider applicability in the application field of brain computer interface. Compared with TSVM, which needs to solve the optimization problem of two SVMS, RSMM only needs to solve the optimization problem of one SMM, and the calculation amount in the optimization calculation process is significantly reduced. Therefore, the proposed method has better practicability in motion image pattern recognition.

5. Conclusions

In this paper, the non-stationary and nonlinear high-dimensional characteristics of the dance motion image EEG signals are analyzed, and the anti-aliasing filtering strategy and parameter optimization method are proposed to achieve pattern recognition of the dance motion image EEG signals. In view of the low spatial resolution of the original EEG signal, the anti-aliasing filtering process can ensure the better resolution of the

two-dimensional empirical wavelet transform features. In addition, according to the variable EEG distribution of different subjects, AF-TDEW can automatically provide suitable RSMM parameters for different EEG distribution for pattern recognition. Compared with traditional methods, the proposed method can improve the recognition accuracy of dance motion imagination. Compared with the deep learning methods, the proposed method achieves almost the same recognition accuracy and requires fewer computational samples and resources, which is more suitable for the application of BCI in the actual environment. The future work will focus on applying the proposed method to actual MI-BCI, further discussing the feature extraction and pattern recognition results of the proposed method according to actual experience, and updating the method and parameters according to the results to make it more suitable for actual application environment.

Acknowledgments. This research received funding by "Study on Inheritance and Development of Yao Umbrella Dance in Lanshan from the perspective of Cultural Ecology. Project number: 22B1029. Project Name: 2022 Scientific Research Project of Education Department of Hunan Province".

References

1. Lecuyer, A., George, L., Marchal, M.: "Toward adaptive VR simulators combining visual, haptic, and brain-computer interfaces," *IEEE computer graphics and applications*, Vol. 33, No. 5, 18-23. (2013)
2. Yin, S., Wang, L., Shafiq, M., et al.: "G2Grad-CAMRL: An Object Detection and Interpretation Model Based on Gradient-weighted Class Activation Mapping and Reinforcement Learning in Remote Sensing Images," *IEEE Journal of Selected Topics in Applied Earth Observations and Remote Sensing*. (2023) doi: 10.1109/JSTARS.2023.3241405.
3. Chen, X., Li, C., Liu, A., et al.: "Toward open-world electroencephalogram decoding via deep learning: A comprehensive survey," *IEEE Signal Processing Magazine*, Vol. 39, No. 2, 117-134. (2022)
4. T. Yu et al., "Enhanced Motor Imagery Training Using a Hybrid BCI With Feedback," in IEEE Transactions on Biomedical Engineering, vol. 62, no. 7, pp. 1706-1717, July 2015, doi: 10.1109/TBME.2015.2402283.
5. L. Yao, N. Jiang, N. Mrachacz-Kersting, X. Zhu, D. Farina and Y. Wang, "Reducing the Calibration Time in Somatosensory BCI by Using Tactile ERD," in IEEE Transactions on Neural Systems and Rehabilitation Engineering, vol. 30, pp. 1870-1876, 2022, doi: 10.1109/TNSRE.2022.3184402.
6. Li H, Ding M, Zhang R, et al. Motor imagery EEG classification algorithm based on CNN-LSTM feature fusion network[J]. Biomedical signal processing and control, 2022, 72: 103342.
7. Liao S C, Wu C T, Huang H C, et al. Major depression detection from EEG signals using kernel eigen-filter-bank common spatial patterns[J]. Sensors, 2017, 17(6): 1385.
8. Zhang Y, Wang Y, Jin J, et al. Sparse Bayesian learning for obtaining sparsity of EEG frequency bands based feature vectors in motor imagery classification[J]. International journal of neural systems, 2017, 27(02): 1650032.
9. Nkengfack L C D, Tchiotsop D, Atangana R, et al. EEG signals analysis for epileptic seizures detection using polynomial transforms, linear discriminant analysis and support vector machines[J]. Biomedical Signal Processing and Control, 2020, 62: 102141.
10. Gao Q, Yang Y, Kang Q, et al. EEG-based emotion recognition with feature fusion networks[J]. International journal of machine learning and cybernetics, 2022, 13(2): 421-429

11. T. Ahmed and L. Longo, "Examining the Size of the Latent Space of Convolutional Variational Autoencoders Trained With Spectral Topographic Maps of EEG Frequency Bands," in IEEE Access, vol. 10, pp. 107575-107586, 2022, doi: 10.1109/ACCESS.2022.3212777.
12. Apicella A, Arpaia P, Mastrati G, et al. EEG-based detection of emotional valence towards a reproducible measurement of emotions[J]. Scientific Reports, 2021, 11(1): 21615.
13. S. Zhang et al., "An Explainable and Generalizable Recurrent Neural Network Approach for Differentiating Human Brain States on EEG Dataset," in IEEE Transactions on Neural Networks and Learning Systems, 2022, doi: 10.1109/TNNLS.2022.3214225.
14. Yuhao Zhao, Hang Li, Shoulin Yin. A Multi-channel Character Relationship Classification Model Based on Attention Mechanism[J]. International Journal of Mathematical Sciences and Computing(IJMSC). vol. 8, no. 1, pp. 28-36, 2022.
15. I. Razzak, M. Blumenstein and G. Xu, "Multiclass Support Matrix Machines by Maximizing the Inter-Class Margin for Single Trial EEG Classification," in IEEE Transactions on Neural Systems and Rehabilitation Engineering, vol. 27, no. 6, pp. 1117-1127, June 2019, doi: 10.1109/TNSRE.2019.2913142.
16. Pan H, Xu H, Zheng J, et al. Multi-class fuzzy support matrix machine for classification in roller bearing fault diagnosis[J]. Advanced Engineering Informatics, 2022, 51: 101445.
17. Houssein E H, Hammad A, Ali A A. Human emotion recognition from EEG-based brainC-computer interface using machine learning: a comprehensive review[J]. Neural Computing and Applications, 2022, 34(15): 12527-12557.
18. Xiao F, Gu L, Ma W, et al. Real time motion intention recognition method with limited number of surface electromyography sensors for A 7-DOF hand/wrist rehabilitation exoskeleton[J]. Mechatronics, 2021, 79:102642.
19. P. Wang, P. Gong, Y. Zhou, X. Wen and D. Zhang, "Decoding the Continuous Motion Imagery Trajectories of Upper Limb Skeleton Points for EEG-Based BrainCComputer Interface," in IEEE Transactions on Instrumentation and Measurement, vol. 72, pp. 1-12, 2023, Art no. 2503212, doi: 10.1109/TIM.2022.3224991.
20. Y. Lin, R. Palaniappan, P. De Wilde and L. Li, "A normalisation approach improves the performance of inter-subject sEMG-based hand gesture recognition with a ConvNet," 2020 42nd Annual International Conference of the IEEE Engineering in Medicine & Biology Society (EMBC), Montreal, QC, Canada, 2020, pp. 649-652, doi: 10.1109/EMBC44109.2020.9175156.
21. Lopes W N, Junior P O C, Aguiar P R, et al. An efficient short-time Fourier transform algorithm for grinding wheel condition monitoring through acoustic emission[J]. The International Journal of Advanced Manufacturing Technology, 2021, 113: 585-603.
22. Ma W, Xue H, Sun X, et al. A novel multi-branch hybrid neural network for motor imagery EEG signal classification[J]. Biomedical Signal Processing and Control, 2022, 77: 103718.
23. Zhang X, Wang T, Xiong Q, et al. A Dense Long Short-Term Memory Model for Enhancing the Imagery-Based Brain-Computer Interface[J]. Computational Intelligence and Neuroscience, 2021, 2021: 1-10.
24. C. Liang and C. Chen, "Generalized Composite Multiscale Diversity Entropy and Its Application for Fault Diagnosis of Rolling Bearing in Automotive Production Line," in IEEE Access, vol. 9, pp. 84545-84558, 2021, doi: 10.1109/ACCESS.2021.3063322.
25. Padmashree A, Krishnamoorthi M. Decision Tree with Pearson Correlation-based Recursive Feature Elimination Model for Attack Detection in IoT Environment[J]. Information Technology and Control, 2022, 51(4): 771-785.
26. Al-Shami T M, Mhemdi A. Approximation operators and accuracy measures of rough sets from an infra-topology view[J]. Soft Computing, 2023, 27(3): 1317-1330.
27. Wang S, Wang H, Perdikaris P. Learning the solution operator of parametric partial differential equations with physics-informed deeponets[J]. Science advances, 2021, 7(40): eabi8605.
28. Mirjalili S, Lewis A. The whale optimization algorithm[J]. Advances in engineering software, 2016, 95: 51-67.

29. https://www.bbci.de/competition/ii/
30. Mirjalili S, Mirjalili S. Genetic algorithm[J]. Evolutionary Algorithms and Neural Networks: Theory and Applications, 2019: 43-55.
31. R. M. Bichara, F. A. Asadallah, M. Awad and J. Costantine, "Quantum Genetic Algorithm for the Design of Miniaturized and Reconfigurable IoT Antennas," in IEEE Transactions on Antennas and Propagation, doi: 10.1109/TAP.2023.3245199.
32. Roy A M. An efficient multi-scale CNN model with intrinsic feature integration for motor imagery EEG subject classification in brain-machine interfaces[J]. Biomedical Signal Processing and Control, 2022, 74: 103496.
33. Li H, Ding M, Zhang R, et al. Motor imagery EEG classification algorithm based on CNN-LSTM feature fusion network[J]. Biomedical signal processing and control, 2022, 72: 103342.
34. Hwaidi J F, Chen T M. Classification of motor imagery EEG signals based on deep autoencoder and convolutional neural network approach[J]. IEEE access, 2022, 10: 48071-48081.
35. Yu Z, Chen W, Zhang T. Motor imagery EEG classification algorithm based on improved lightweight feature fusion network[J]. Biomedical Signal Processing and Control, 2022, 75: 1036

Tianliang Huang is with the School of Art; Hunan University of Information Technology; Maotang Industrial Park, Changsha Economic and Technological Development Zone (410151). Research direction: Research on folk dance, image processing.

Ziyue Luo is with the School of Art; Hunan University of Information Technology; Maotang Industrial Park, Changsha Economic and Technological Development Zone (410151). Research direction: Research on folk dance, image processing.

Yin Lyu is with College of Music, Huaiyin Normal University, Huaian, China. His research direction is musical emotion analysis.

Received: December 22, 2022; Accepted: June 01, 2023.